Journal of Electronic Imaging 8(4), 332–341 (October 1999).

Spectral imaging by a multichannel camera

Shoji Tominaga
Osaka Electro-Communication University
Department of Engineering Informatics
Neyagawa, Osaka 572-8530, Japan
E-mail: shoji@tmlab.osakac.ac.jp

Abstract. *A set of multichannel camera systems and algorithms is described for recovering both the surface spectral-reflectance function and the illuminant spectral-power distribution from the data of spectral imaging. We describe a camera system with six spectral channels of fixed wavelength bands. This system is composed of a monochrome charge-coupled device camera, six different color filters, and a personal computer. The dynamic range of the camera is extended for sensing the high-intensity levels of highlights. We assume that the object surfaces in a scene are made of an inhomogeneous dielectric material whose reflection properties are described by the dichromatic reflection model. The process for estimating the spectral data comprises several steps: (1) finite-dimensional linear model representation of wavelength functions, (2) illuminant estimation, (3) data normalization and image segmentation, and (4) reflectance estimation. An algorithm is proposed for detecting highlight areas in the image. The reliability of the camera system and the algorithms is demonstrated in an experiment. Finally, a new type of camera system using a liquid-crystal filter is proposed.* © *1999 SPIE and IS&T.* [S1017-9909(99)00504-8]

1 Introduction

Spectral information such as the spectral-power distribution of illumination and the surface-spectral reflectances of objects is represented as a function of wavelength in the visible region of 400–700 nm. Knowledge of these spectral functions is crucial for realizing color constancy,[1,2] accurate color reproduction,[3] and rendering realistic images.[4] The normal imaging system using a charge-coupled device (CCD) camera with red, green, and blue channels often has difficulty in estimating the spectral functions because illuminants and surface reflectances in natural scenes are spectrally multidimensional. A multichannel camera with more than three spectral bands provides an effective imaging device to estimate the complicated shapes of the surface and illuminant functions.

The present paper describes a set of camera systems and algorithms for recovering the surface-spectral reflectance function and the illuminant spectral-power distribution from image data. We consider multichannel camera systems with different types of filtering mechanisms. A typical system uses color filters with fixed wavelength bands. In a previous paper[5] we proposed the basic system of a multichannel camera with six spectral channels using color filters. Improvements were made on several points.[6] The second generation of a six-channel camera system for practical use is described in this paper. The spectral channels are created by combining a monochrome CCD camera with (a) six different color filters to sample the spectrum, and (b) a specially designed shutter to extend the dynamic range of the camera sensors. The spectral sensitivity of each sensor is calibrated, and the dynamic range is extended to sense a wide range of intensity levels including those of highlights. The spectral channels are defined by the six wavelength bands of the color filters. In the future, a tunable liquid-crystal filter will provide a more convenient type of filtering mechanism since variable spectral channels can be realized.

Some features of the present study on estimating spectral information can be summarized as follows:

1. Light reflection from an object surface is described by the dichromatic reflection model.[7] When we assume that the surface of an object is made of inhomogeneous dielectric material, this model suggests that light reflected from the surface of an inhomogeneous dielectric object is composed of two additive components, the body reflection and the interface reflection.[8] The dichromatic reflection model is valid for many materials including plastic, oil, and water paints.

2. The unknown spectral functions of the illuminant spectral-power distribution and the surface-spectral reflectance are described by linear finite-dimensional models.[1] These models suggest that the continuous spectral functions are expressed as linear combinations of several basis functions. In fact, it is known that light sources (except for fluorescent lamps) and most reflectances of natural and artificial objects can be described by low-dimension linear models.[9–11]

3. The two kinds of spectral functions are estimated in two steps. First, the illuminant spectral-power distribution is estimated from the image data for highlight regions within separate objects. Second, the spectral reflectance is estimated based on two-dimensional histogram analysis of the corrected image data for each surface.

In this paper we present several proposals concerning the following points:

This paper is a revision of a paper presented at the SPIE conference on Color Imaging; Device-Independent Color, Color Hardcopy, and Graphic Arts IV, San Jose, CA, January 1999. The paper appears (unrefereed) in *Proc. SPIE* **3648**.

Paper 005904 received Mar. 17, 1999; revised manuscript received May 13, 1999; accepted May 18, 1999.
1017-9909/99/$10.00 © 1999 SPIE and IS&T.

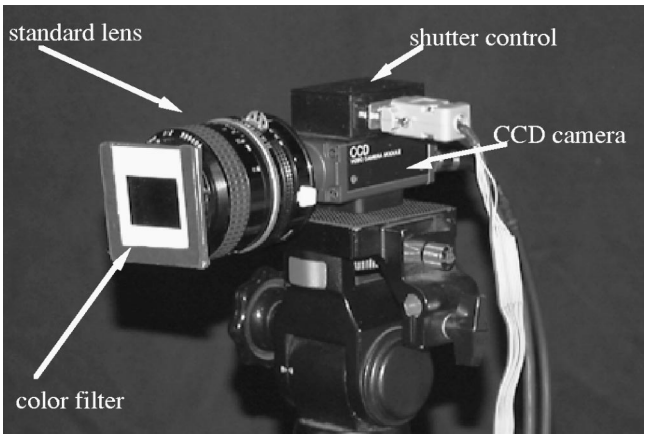

Fig. 1 Six-color camera system.

1. In order to obtain more reliable image data, we have built a new camera system with six spectral channels. In contrast to the previous camera system which was based on a coarse resolution of an 8 bit image quantization and on coarse measurement results for the spectral-sensitivity functions, we present a system using a new camera with improved spectral resolution and accurate spectral sensitivities.

2. We have improved the method for estimating surface-spectral reflectance. The previous estimation results suffered from the problem of instability caused by noisy fluctuations in the measurements. An improved algorithm has been developed to solve this problem.

3. Algorithms are presented for processing the six-dimensional image data from the initial measurement all the way to the final estimation. We also introduce unique algorithms for highlight detection and region segmentation.

4. We present a new type of camera system using liquid-crystal filters. While the six-color camera system has six spectral channels of fixed wavelength bands, a tunable liquid-crystal filter is more convenient for spectral imaging in the sense of being able to easily change the wavelength band.

In the following, Sec. 2 describes the six-color camera system. Section 3 describes the finite-dimensional linear model and the modeling of camera outputs. Section 4 describes the method for estimating the spectral parameters for illuminant and spectral reflectances. Practical estimation procedures and some experimental results are presented in Secs. 5 and 6, respectively. We introduce briefly a new type of camera system using liquid-crystal filters in Sec. 7.

2 Six-color Camera System

2.1 *System Construction*

Figure 1 shows the camera system used in the present study. It is the second generation of a six-channel camera for spectral imaging that includes some improvements compared with the previous system.[5] The camera system is composed of a monochromatic CCD camera (Sony model XC-75), a standard photographic lens (Nikon Nikkor 35 mm F1.4S), color filters (Kodak Wratten gelatin filters), and a personal computer.

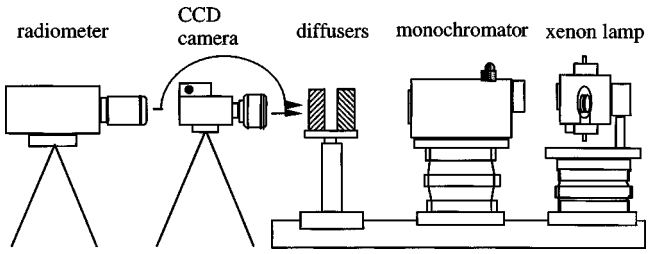

Fig. 2 Setup for measuring the spectral sensitivity of the monochrome CCD camera.

To extend the dynamic range of the CCD camera, we use different shutter speeds in conjunction with a fixed aperture size. A mechanism is implemented for changing the shutter speed under computer control. Moreover, a 10 bit frame grabber is used to improve the resolution of intensity quantization, so that the monochrome camera signal is quantized to 10 bits of intensity, resulting in a digital signal with 1024 levels.

2.2 *System Characteristics*

2.2.1 *Spectral-sensitivity function*

Accurate knowledge of the spectral-sensitivity function for each sensor of the multichannel camera system is needed for estimating the illuminant spectrum and the surface-spectral reflectance. In the previous study,[5] we measured the spectral sensitivity of the monochrome CCD camera by using a set of 31 interference filters. The interference filters convert the continuous light spectrum of a lamp into a set of narrow bandwidth light spectra; strictly speaking, these filtered light spectra do not represent monochromatic light, as each spectrum has a bandwidth of 9–20 nm. In the present study a monochromator is used for precise measurement of the spectral sensitivity of the camera.

Figure 2 shows the setup for measuring the spectral sensitivity of the CCD camera. The monochromator converts the continuous spectrum of a xenon lamp into a set of 61 equally spaced monochrome wavelengths throughout the visible wavelength range of 400–700 nm. The monochromatic light is then guided to diffusers, and the diffused light is measured with both the camera and the radiometer. The spectral-sensitivity function of the camera is determined as the ratio of the camera output to the measured radiance at each of the 61 wavelengths. Figure 3 shows the spectral sensitivity functions for the six sensors which are a combination of the spectral-sensitivity function of the camera and the spectral transmittances of the different color filters. Thus, the visible wavelength region is decomposed into six bands, and the spectral image corresponding to each band is measured by the camera system. This is the reason why this system is called a six-color camera.

2.2.2 *Noise reduction*

To reduce the effect of random noise, pictures of the same scene are taken eight times, and these pictures are averaged on a frame grabber as the measured image. The noise level is then reduced to $1/\sqrt{8}$. Moreover, in order to discount the

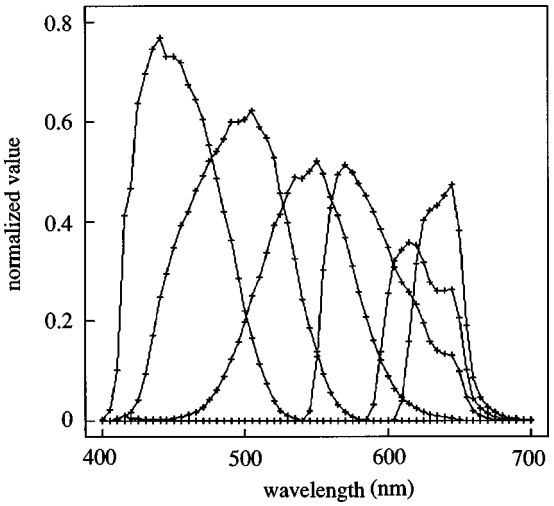

Fig. 3 Spectral sensitivity functions of the six-color camera.

dark current of the CCD sensor, an offset image taken with a closed shutter is subtracted from the measured image with the same exposure time.

2.2.3 *Dynamic range extension*

We have to sense a wide intensity variation on object surfaces ranging from matte parts to highlight parts for highlight estimation. The dynamic range of 10 bits for image intensity is often insufficient for this purpose. If the incoming light from a strong highlight exceeds the range of [0, 1023], then the CCD elements saturate. To solve this problem, we take multiple pictures of the same scene by using different shutter speeds, and combine the multiple images into a single image, so that the dynamic range is extended.

For example, consider three pictures taken at shutter speeds of 1/125th, 1/250th, and 1/500th of a second, respectively, i.e., three exposure times of 8, 4, and 2 ms, in 1/2 steps. Let 1/125 s be the standard shutter speed. Moreover let p_{ij} and $p_{ij}^{(k)}$ indicate the (i,j) pixel values, respectively, in the combined image and in the k ms image. First, if $p_{ij}^{(8)}<1023$, then the output is $p_{ij}=p_{ij}^{(8)}$. Second, if $p_{ij}^{(8)}=1023$ and $p_{ij}^{(4)}<1023$, then we discard $p_{ij}^{(8)}$ and accept $p_{ij}^{(4)}$ as $p_{ij}=2\times p_{ij}^{(4)}$. Third, if $p_{ij}^{(4)}=1023$ and $p_{ij}^{(2)}<1023$, then $p_{ij}=4\times p_{ij}^{(2)}$. This procedure provides a combined image with the extended range [0, 4095].

Note that a good linearity in the camera response is required to perform this operation. To examine the linearity, color patches were measured with both the camera and a radiometer. By a comparison of the camera outputs with the luminances of the incident light, the present camera was determined to have a good linearity of $\gamma=1$ without saturation.

3 Models of Spectral Functions and Camera Outputs

3.1 *Color Signals and Spectral Functions*

Light reflected from an object surface and entering the camera lens, $C^o(x,\lambda)$, called the color signal, is a function of the wavelength λ and the location parameter x, including various geometric parameters under a fixed imaging geometry. The symbol o indicates an object number. The dichromatic reflection model suggests that the color signal from the surface of an inhomogeneous dielectric object is composed of two additive components, the body reflection and the interface reflection.[7,8] The color signal $C^o(x,\lambda)$ is then expressed in the form

$$C^o(x,\lambda)=\alpha(x)S^o(\lambda)E(\lambda)+\beta(x)E(\lambda), \tag{1}$$

where $S^o(\lambda)$ is the surface-spectral reflectance function of an object o, and $E(\lambda)$ is the spectral-power distribution of the illumination. The first term on the right-hand side in Eq. (1) represents the body reflection, where $\alpha(x)$ is its shading factor, while the second term represents the specular reflection, where $\beta(x)$ is the scale factor.

We use linear finite-dimensional models to describe the spectral functions. These models are effective in the sense that the number of unknown parameters in the spectral functions estimation can be reduced significantly when spectral functions with continuous spectra are represented by only a small number of basis functions. Specifically, we assume that the illuminant $E(\lambda)$ can be expressed as a linear combination of m basis functions as

$$E(\lambda)=\sum_{i=1}^{m}\epsilon_i E_i(\lambda), \tag{2}$$

where $\{E_i(\lambda),\ i=1,2,...,m\}$ is a statistically determined set of basis functions for the illuminant, and $\{\epsilon_i\}$ is a set of scalar weights. We also suppose that the spectral reflectance function $S^o(\lambda)$ can be expressed in the same fashion with n reflectance basis functions as

$$S^o(\lambda)=\sum_{i=1}^{n}\sigma_i^o S_i(\lambda), \tag{3}$$

where $\{S_i(\lambda),\ i=1,2,...,n\}$ is the set of basis functions for the reflectance, and $\{\sigma_i^o\}$ is the set of weights.

The numbers of basis functions m and n define the model dimensions for illuminant and surfaces, respectively. Because the basis functions are known, given the above formulation in terms of linear models, the estimation problem becomes one of inferring two sets of weight coefficients $\{\epsilon_i\}$ and $\{\sigma_i^o\}$ from the camera outputs. As we use six spectral bands, the model dimensions m and n are bounded to be six or less.

3.2 *Camera Outputs*

The spectral image consists of six sensor outputs at each spatial location x. The color signal $C^o(x,\lambda)$ and the sensor spectral-sensitivity functions $R_i(\lambda)$ are related to the outputs $\rho_i^o(x)$ by the equation

$$\rho_i^o(x)=\int C^o(x,\lambda)R_i(\lambda)\,d\lambda, \quad i=1,2,...,6. \tag{4}$$

The shapes of the above spectral-sensitivity functions are shown in Fig. 3.

We summarize the imaging relationships between the sensor responses and the illuminant and surface functions in a matrix form. First, define six-dimensional vectors $\mathbf{h}_i$ $(i=1,2,...,m)$ representing the sensor responses for the illuminant basis as

$$\mathbf{h}_i=\left[\int E_i(\lambda)R_1(\lambda)\mathrm{d}\lambda,\ldots,\int E_i(\lambda)R_6(\lambda)\mathrm{d}\lambda\right]^t,\quad i=1,2,...,6, \tag{5}$$

where the symbol t has the meaning of a matrix transposition. These sensor responses are summarized in a 6-by-m matrix $\mathbf{H}$

$$\mathbf{H}=[\mathbf{h}_1,\mathbf{h}_2,\ldots,\mathbf{h}_m]=\begin{bmatrix} h_1 & h_{12} & \cdots & h_{1m} \\ \vdots & \vdots & & \vdots \\ h_{61} & h_{62} & \cdots & h_{6m}\end{bmatrix}. \tag{6}$$

Next, define a 6-by-n matrix $\mathbf{\Lambda}_{\boldsymbol{\epsilon}}$ representing the sensor response for the color basis whose (i,j) element is defined as

$$[\mathbf{\Lambda}_{\boldsymbol{\epsilon}}]_{ij}=\sum_{k=1}^{m}\epsilon_k\int E_k(\lambda)S_j(\lambda)R_i(\lambda)\mathrm{d}\lambda. \tag{7}$$

Substituting the finite-dimensional model expressions for $E(\lambda)$ and $S^o(\lambda)$ into Eq. (4) and using the above matrix notations permits us to express the general imaging relationship between the sensor outputs and the scene parameters as the vector equation

$$\boldsymbol{\rho}^o(x)=\alpha(x)\mathbf{\Lambda}_{\boldsymbol{\epsilon}}\boldsymbol{\sigma}^o+\beta(x)\mathbf{H}\boldsymbol{\epsilon}, \tag{8}$$

where $\boldsymbol{\rho}^o(x)$ is a column vector formed from six sensor responses $\rho_k^o(x)$ $(k=1,2,...,6)$. The vectors $\boldsymbol{\sigma}^o$ and $\boldsymbol{\epsilon}$ are of dimensions n and m, respectively, and they represent the weight vectors for surface reflectance and illuminant.

4 Estimation Method of Spectral Parameters

The dichromatic imaging model defined in Eq. (8) shows that the sensor output $\boldsymbol{\rho}^o(x)$ for any spatial location x of an object is expressed as a linear combination of the two reflection component vectors $\mathbf{\Lambda}_{\boldsymbol{\epsilon}}\boldsymbol{\sigma}^o$ and $\mathbf{H}\boldsymbol{\epsilon}$. These two vectors span a two-dimensional subspace (plane) in the six-dimensional sensor space, and all the camera outputs observed from the same object surface fall in this subspace. This subspace is called the *color-signal plane* $P^{(o)}$. We note that the vector $\mathbf{\Lambda}_{\boldsymbol{\epsilon}}\boldsymbol{\sigma}^o$ is not only a function of the parameter $\boldsymbol{\sigma}^o$, but also the illumination parameter $\boldsymbol{\epsilon}$ that is included in $\mathbf{\Lambda}_{\boldsymbol{\epsilon}}$. On the other hand, the vector $\mathbf{H}\boldsymbol{\epsilon}$ is a function of only the illumination parameter.

Therefore, the parameter estimation is performed in two steps. First we estimate the parameter $\boldsymbol{\epsilon}$ and recover the illumination. Second, we estimate $\boldsymbol{\sigma}^o$ and recover the body reflectance function. To estimate the body reflectance function we must remove the effect of illumination and segment the image into uniform surface areas.

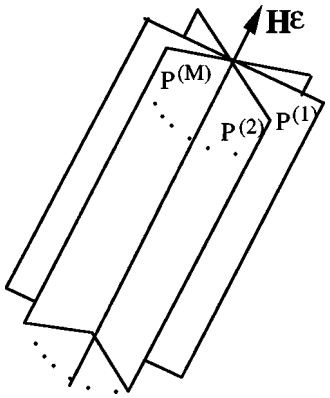

Fig. 4 Intersection of color-signal planes.

4.1 *Illuminant Estimation*

The illuminant parameters can be estimated from the interface reflection component of the color signals. Because the interface reflection is common to all color signals for different surfaces, this component is extracted as a common vector component to different color-signal planes. Suppose that the image sensors observe M objects illuminated with one light source, and the areas with high intensity are extracted from the image data. The M color-signal planes must intersect because $\mathbf{H}\boldsymbol{\epsilon}$ is contained in all planes $P^{(1)},P^{(2)},\ldots,P^{(M)}$ as shown in Fig. 4. Once the intersection is found, the illuminant vector $\boldsymbol{\epsilon}$ is recovered by applying a matrix inversion $\mathbf{H}^{-1}$ or a pseudomatrix inversion $\mathbf{H}^{+}$ to $\mathbf{H}\boldsymbol{\epsilon}$.

Concerning the intersection determination, Tominaga and Wandell[8] presented an algorithm for finding the intersection of two planes for the case of two objects. Tominaga[5] extended this algorithm to find a reliable estimate of the common intersection of planes for the general case of two or more objects. Let M pairs of vectors $[\mathbf{u}_1^{(1)},\mathbf{u}_2^{(1)}]$, $[\mathbf{u}_1^{(2)},\mathbf{u}_2^{(2)}],\ldots,[\mathbf{u}_1^{(M)},\mathbf{u}_2^{(M)}]$ be the orthonormal bases that define the planes $P^{(1)},P^{(2)},\ldots,P^{(M)}$, respectively. The basis vectors can be obtained computationally from the singular-value decomposition (SVD) of the observed data. The intersection line must lie in all M planes and be expressed in a linear combination of the basis vectors $\mathbf{u}_1^{(i)}$ and $\mathbf{u}_2^{(i)}$ $(i=1,2,...,M)$. Therefore, a reliable estimate of the intersection vector $\mathbf{e}$ is given as a form of the mean value

$$\mathbf{e}=\frac{1}{M}\sum_{i=1}^{M}(c_1^{(i)}\mathbf{u}_1^{(i)}+c_2^{(i)}\mathbf{u}_2^{(i)}). \tag{9}$$

The detailed method for calculating the coefficients $c_1^{(i)}$ and $c_2^{(i)}$ is shown in Ref. 5.

Even without using multiple surfaces, it is possible to estimate illuminant from a single specular surface. Tominaga[12] developed an algorithm to predict the illuminant spectrum from a single surface of an inhomogeneous dielectric object. This algorithm uses the property that the distribution of the observed color signals is composed of two linear clusters in the sensor space: the body cluster and the interface cluster. When the viewing direction to object

surfaces is almost coincident with the illumination direction, the illuminant spectrum can be estimated from the principal component vector of the interface cluster. However, the illuminant estimation can be made even more reliably by using multiple surfaces.

The above algorithms for illuminant estimation may be compared with other methods such as the subspace method by Maloney and Wandell[13] and the Bayesian method by Brainard and Freeman.[14] The subspace method is not available for object surfaces having the dichromatic reflection property, but for diffusely reflective surfaces. The Bayesian method is based on a statistical assumption that illuminant spectral-power distributions obey a multivariate normal distribution. On the other hand, the present algorithms have no assumption on illuminant statistics.

4.2 *Elimination of Illumination Effect*

To estimate the body reflectance function of the surface in the image, we must remove the effects of specularity and shading, and then segment the image into uniform surface areas.

First of all, the influence of illumination is reduced from the sensor outputs as

$$y_i(x)=\rho_i(x)/\hat{e}_i, \quad i=1,2,...,6, \tag{10}$$

where $\hat{\mathbf{e}}\equiv[\hat{e}_1,\hat{e}_2,\ldots,\hat{e}_6]^t$ is an estimate of the illuminant vector $\mathbf{H}\boldsymbol{\epsilon}$. The above division means an operation in the form $y_i(x)=\alpha(x)(\Lambda_\epsilon\sigma^o/\mathbf{H}\boldsymbol{\epsilon})_i+\beta(x)$, where $(\Lambda_\epsilon\sigma^o/\mathbf{H}\boldsymbol{\epsilon})_i$ is done elementwise. If the spectral-sensitivity functions are narrow bands, the vector $\mathbf{y}(x)\equiv[y_1,y_2,\ldots,y_6]^t$ is independent of illumination.

Next, this modified sensor output $\mathbf{y}(x)$ is normalized to eliminate the constant interface reflection term and the geometric factors $\alpha(x)$ and $\beta(x)$. This normalization process consists of two steps: First, define a deviation vector as $y_i(x)-\overline{y}(x)$, where $\overline{y}(x)$ denotes the average over the six sensor outputs. In this step the interface reflection term $\beta(x)$ is deleted. Second, normalize the deviation vector to a unit length vector as

$$\tilde{y}_i(x)=(y_i(x)-\overline{y}(x))\Big/\sqrt{\sum_{j=1}^{6}(y_j(x)-\overline{y}(x))^2}, \quad i=1,2,...,6. \tag{11}$$

Here, the geometric factor $\alpha(x)$ to the deviation vectors is then canceled out.

Thus, the normalized sensor output $\tilde{\mathbf{y}}(x)\equiv[\tilde{y}_1,\tilde{y}_2,\ldots,\tilde{y}_6]^t$ is independent of the vector $\mathbf{H}\boldsymbol{\epsilon}$, and the scalars $\alpha(x)$ and $\beta(x)$, so that this vector depends mostly on the body reflectance of an object surface.

This normalization property permits us to classify the sensor outputs on the basis of different surface materials in a scene. In other words, we can segment the image into uniform surface areas. Figure 5 shows an example of histogram characteristics resulting from the above normalization of the image data. Suppose that three objects A, B, and C are illuminated by a single light source as shown in Fig. 5(a). Figure 5(b) shows the original histogram of the camera data for the three objects in a three-dimensional space.

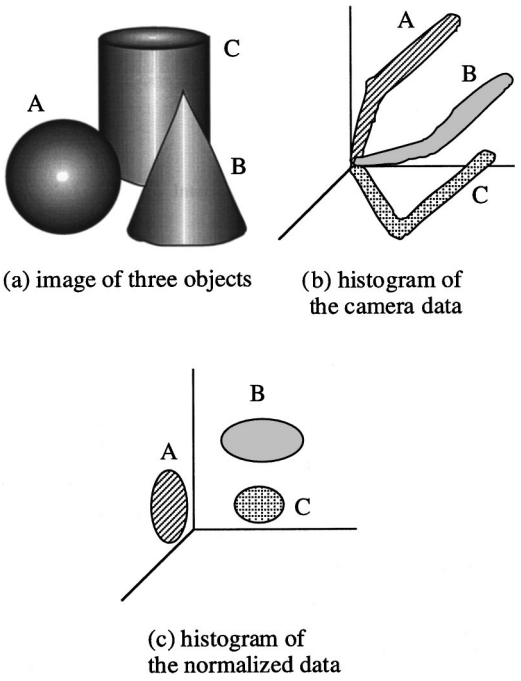

Fig. 5 Normalization of the camera data and histogram characteristics.

Because of the property of dichromatic reflection, each histogram is depicted as the shape of a skewed L, which is composed of two linear clusters: the body cluster and the interface cluster. After deleting the illumination effect, the normalization of $\tilde{\mathbf{y}}(x)$ forms dense clusters as shown in Fig. 5(c). Therefore, we detect the dense clusters A, B, and C based on a histogram analysis in the space, so that we can segment the image and extract the corresponding three uniform surface areas.

In comparison with previous color constancy methods, from an image segmentation point of view it should be noted that linear space methods are not always used in surface segmentation. For example, the Maloney–Wandell method does not take surface segmentation into account. It assumes that the sensor responses come from a single object surface, that is, object surfaces are segmented in advance.

4.3 *Reflectance Estimation*

For each area in the segmented image, we estimate a unique reflectance function from the classified sensor outputs as one surface. The sensor outputs are analyzed on the color-signal plane. Because of the two-dimensionality, the body reflection vector $\mathbf{\Lambda}_\epsilon\boldsymbol{\sigma}^o$ can be expressed in terms of two orthonormal vectors $[\mathbf{H}\boldsymbol{\epsilon}]$ and $[\mathbf{H}\boldsymbol{\epsilon}]^\perp$ as

$$\mathbf{\Lambda}_\epsilon\boldsymbol{\sigma}^o=c_e[\mathbf{H}\boldsymbol{\epsilon}]+c_\epsilon^\perp[\mathbf{H}\boldsymbol{\epsilon}]^\perp, \tag{12}$$

where $[\mathbf{H}\boldsymbol{\epsilon}]$ was obtained as the estimate in Sec. 4.1, and $[\mathbf{H}\boldsymbol{\epsilon}]^\perp$ is a unit length vector perpendicular to $[\mathbf{H}\boldsymbol{\epsilon}]$ on the plane $P^{(o)}$. Scalars c_e and $c_e^\perp$ are the weighting coefficients. A permissible solution for the coefficients is given by applying an extended quarter-circle analysis.[2,15]

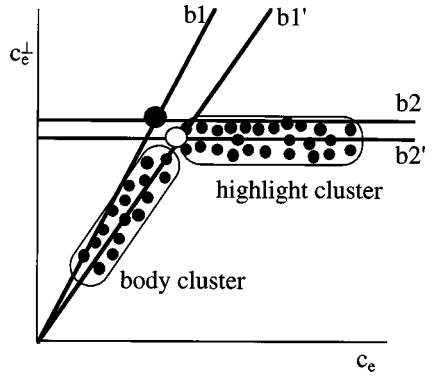

Fig. 6 Distribution of coefficients $(c_e, c_e^\perp)$ on the image signal plane and estimation of the unknown weights.

Figure 6 demonstrates the coordinate system of $(c_e, c_e^\perp)$. Each dot indicates the observation to location x on a surface in this transformed coordinate frame. The c_e axis represents the weight of the interface reflection, that is, the illumination, while the $c_e^\perp$ axis represents the contribution due to the body reflection. In the previous study[2,15] we determined an estimate of the vector $\mathbf{\Lambda}_\epsilon \boldsymbol{\sigma}^o$ as the data point of sensor responses on the plane that was farthest away from the illuminant vector **e**. In Fig. 6, the estimate is given at an intersection between boundaries $\mathbf{b}_1$ and $\mathbf{b}_2$ as shown with the filled circle.

However, a detailed inspection has suggested that the above estimate is influenced by noisy fluctuation in measurements. In fact, note that the intersection point between $\mathbf{b}_1$ and $\mathbf{b}_2$ is determined by only two observations, so that the coordinates are unstable. The camera outputs are two-dimensional in principle from the dichromatic reflection property, that is, the distribution of pixels is two-dimensional in a color-signal plane. However, if the camera views a scene in the same direction of illumination, the pixel distribution is not widely scattered in the plane, but forms two linear clusters as shown in Fig. 6.

For this reason, we propose to determine an intersection between the axes of principal components for two clusters. As shown by an open circle in Fig. 6, the intersection between the component axis $\mathbf{b}_1'$ for the body cluster and the component axis $\mathbf{b}_2'$ for the highlight axis is determined as an estimate of $\mathbf{\Lambda}_\epsilon \boldsymbol{\sigma}^o$. We denote this coordinate point as the symbol $(\hat{c}_e, \hat{c}_e^\perp)$. Finally, the estimate of the reflectance parameter $\boldsymbol{\sigma}^{\mathbf{o}}$ is given as

$$\hat{\boldsymbol{\sigma}}^o = \mathbf{\Lambda}_\epsilon^+ (\hat{c}_e[\mathbf{H}\boldsymbol{\epsilon}] + \hat{c}_e^\perp[\mathbf{H}\boldsymbol{\epsilon}]^\perp), \tag{13}$$

where $\mathbf{\Lambda}_\epsilon^+$ is the n-by-6 pseudoinverse of $\mathbf{\Lambda}_\epsilon$.

5 Image Processing

5.1 *Highlight Extraction*

By the dichromatic reflection property, highlight parts of object surfaces must provide us with useful information on illumination. High-luminance regions including highlights are extracted for estimating illuminant spectrum from the six-dimensional image data. Here, we propose a method for extracting highlights on the basis of the CIE *XYZ* color-specification system.

5.1.1 *Acquisition of tristimulus values*

Because the spectral-sensitivity functions of the six-color camera are given as shown in Fig. 3, the tristimulus values *XYZ* at each pixel can be calculated from the camera output. First, the spectral-sensitivity functions $R_i(\lambda)$ $(i = 1,2,...,6)$ are fitted to the CIE color-matching functions $\overline{x}(\lambda)$, $\overline{y}(\lambda)$, and $\overline{z}(\lambda)$ in the method of least squares. The coefficients in this fitting are summarized into a 3×6 transformation matrix **M**. The *XYZ* values are then obtained as the following linear transformation:

$$\begin{bmatrix} X \\ Y \\ Z \end{bmatrix} = \mathbf{M}\rho, \tag{14}$$

where the Y value represents luminance, and the chromaticity coordinates (x,y) are calculated by

$$x = X/(X+Y+Z), \quad y = Y/(X+Y+Z). \tag{15}$$

Thus, a set of the color coordinates (Y,x,y) is obtained at each pixel in the entire image.

5.1.2 *Detection of high-luminance regions*

Bright regions in the image are detected on the luminance Y. When highlights occur on different object surfaces, use of only a single threshold based on the Y value is insufficient for detecting all the highlights. This is because the luminance of the highlight on an object surface always depends on the body color. Therefore, we first detect regions brighter than a certain luminance level in the image, and second, determine a highlight part within each detected area. In the first step the bright regions are extracted as a set of pixels satisfying the condition

$$Y > \overline{Y} + k_1 S, \tag{16}$$

where $\overline{Y}$ is the average value for all pixels, S is the standard deviation, and k_1 is a parameter for decision.

5.1.3 *Deletion of small regions*

The number of pixels is counted in each closed area with connected pixels. Regions smaller than a certain area are neglected in the estimation procedure from the standpoint of reliability. Moreover, we neglect a single highlight even though the area is large. The single highlight means an isolated highlight or a pseudohighlight by noise. We regard a region as the single highlight region if the pixel with the highest luminance $Y_{\max}$ in the region is isolated, and there is no pixel with the succeeding high luminance to $Y_{\max}$ in the neighborhood.

5.1.4 *Determination of highlight regions*

A set of pixels looking white is searched in each of the remaining regions. Let $(x_{\max}, y_{\max})$ be the chromaticity coordinates of a pixel with $Y_{\max}$ in each area. Then, pixels

with similar chromaticity are detected in the neighborhood of the maximum point. That is, a set of highlight pixels is determined so that the chromaticity (x,y) satisfies the condition

$$\sqrt{(x-x_{\max})^2+(y-y_{\max})^2}<k_2, \tag{17}$$

where k_2 is a parameter.

5.2 *Determination of Basis Functions*

To derive the illuminant basis functions, we have used a set of nine spectra from CIE standard illuminants and several real sources. The data set consists of (1) CIE standard illuminants A, B, and C; and (2) CIE daylights D_{55}, D_{65}, and D_{75}; and (3) our set of the measured spectra from sunlight, a slide projector, and a tungsten–halogen lamp. Principal component patterns are extracted from the SVD of the set of nine spectra. The basis functions are determined according to the percent variance of the component vectors. A statistical method for deciding the linear model dimension of the illuminant is shown in Ref. 4. In the present study, we select the first three principal components as the basis functions of the three-dimensional model of $m=3$.

The reflectance basis functions are determined using a database of surface-spectral reflectances provided by the Eastman Kodak Company.[12] This database consisted of 354 measured reflectance spectra of different materials collected from Munsell chips, paint chips, and natural objects. We determine the reflectance basis functions $\{S_i(\lambda)\}$ based on the direct SVD of these spectra. The percent variance accounted for is 0.998 for the first five components. Our experimental results have shown that the five-dimensional model of $n=5$ gives the most appropriate dimension for minimizing the error of reflectance estimation.

5.3 *Image Segmentation*

The image segmentation is done as a preprocessing of surface-spectral reflectance estimation by means of cluster detection in the six-dimensional space of the normalized vector $\tilde{\mathbf{y}}(x)$. Dense clusters corresponding to uniform surface regions are detected from a histogram analysis in the space. This detection process is similar to the cluster detection of partitioning a color image into a set of uniform color regions. The basic process is based on sequential cluster detection in a three-dimensional color space. The author[16] previously presented the detection algorithm by an iterative analysis of a one-dimensional histogram in a uniform color space. However, this algorithm is limited to a three-dimensional color space. Therefore, we have developed a cluster detection algorithm working in a six-dimensional space based on the same principle as the three-dimensional one, so that the algorithm can segment the six-dimensional image into uniform surface areas with the same spectral reflectance.

6 *Experimental Results*

Figure 7 shows the scene of a plastic toy car. This object was illuminated with an incandescent lamp (500 W) at a distance of 1.5 m. The camera was placed so that the viewing direction was almost coincident with the illumination direction. The object is composed of 12 parts in five colors: red, green, blue, yellow, and white. The image size is 369 $\times$257. In addition to the six-color camera, a spectroradiometer was used to obtain direct measurements of the illuminant spectral-power distribution and the surface-spectral reflectances of the plastic objects.

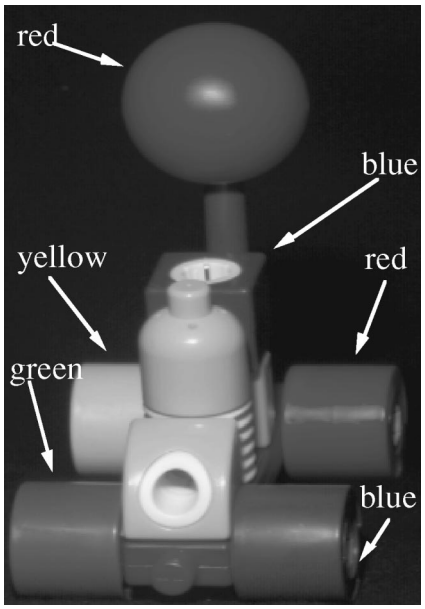

Fig. 7 Scene of measuring a toy car.

Figure 8 shows the extraction results of highlight regions from the six-dimensional image, where Fig. 8(a) indicates the regions with high luminance Y. Almost all the bright regions in the original scene are detected with $k_1=0.5$, and these are painted black. Note that three yellow surfaces and a white surface are detected as a single large region because these surfaces are connected to each other in the image. In this large region, very few highlight pixels are in the neighborhood of the maximum luminance pixel. Therefore, we have discarded this region from highlight regions. Figure 8(b) indicates the resulting highlight re-

Fig. 8 Extraction results of highlight areas. (a) High-luminance regions and (b) highlight regions.

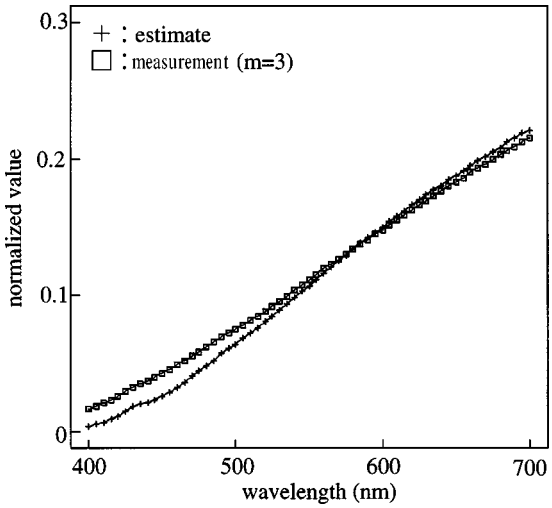

Fig. 9 Estimation results of illuminant.

gions within the chromaticity limit of $k_2 = 0.06$. Several white regions on the red ball, the red wheel, the green wheel, and the blue wheel are extracted as highlights.

The illuminant estimation was done using these four regions. Figure 9 shows the estimation results, where the illuminant estimate from the image data is represented by a solid line marked with plus symbols. The illuminant distribution measured directly by the spectroradiometer is represented with open squares in the figure, where the measured spectrum is described by the three-dimensional linear model

$$E(\lambda) = \sum_{i=1}^{3} \epsilon_i E_i(\lambda).$$

The estimated spectrum reproduces well the feature of being a linear spectrum for the incandescent illuminant distribution, although a certain discrepancy is found in the range of the short wavelength.

Next, the normalized data of $\tilde{\mathbf{y}}$ without the influence of illumination were calculated for all the pixels except for a dark background. Several dense clusters were detected based on the histogram in the six-dimensional space, and the image was segmented into several regions. Figure 10 shows the segmentation results, where the object surfaces are segmented into six color regions. The color numbers shown in the figure correspond to (1) red, (2) yellow, (3) blue, (4) green, (5) white, and (6) gray (hole). Considering the connectivity of the regions, we can see that the image is partitioned into ten connected regions.

Finally, the surface-spectral-reflectance functions were estimated for the regions with a large area. Figure 11 shows the reflectance estimation results for the four regions of yellow, green, red (wheel), and blue (wheel), where the plus symbols represent the estimates from the image data by the proposed method, diamonds represent the five-dimensional model of the measured spectral reflectances, and the open squares represent the estimates by the previous method using the quarter-circle analysis.[2,15] All the spectral curves are expressed in values relative to a standard so that the maximum reflectance of yellow is set to 1.

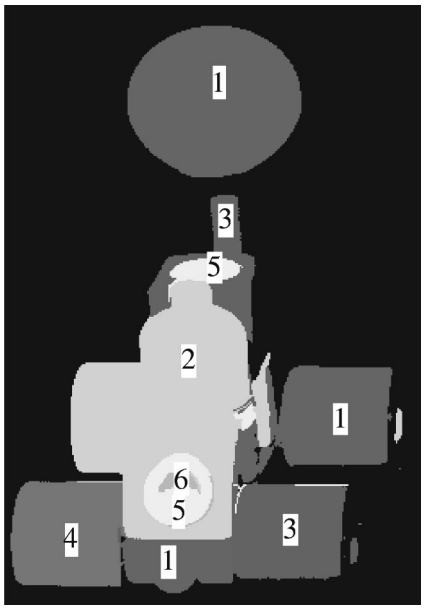

Fig. 10 Segmentation results by cluster detection.

A comparison among the three curves for each surface indicates the reliability of the reflectances estimated by the proposed method.

7 Spectral Imaging by a New Type of Filtration Mechanism

The six-color camera system in the previous sections has six spectral channels of the color filter's fixed wavelength bands. The filtration for each channel depends mostly on the transmittances of color filters, and partly on the spectral sensitivity of a monochrome camera. It should be noted that the selection of color filters is very limited, and filters with a narrow bandpass are difficult to make. Therefore, a camera system using the present filtration mechanism has the difficulty that both increasing the number of channels and exchanging the filters are not easy.

Here, we propose a camera system based on a new filtration mechanism using a tunable liquid-crystal filter. This

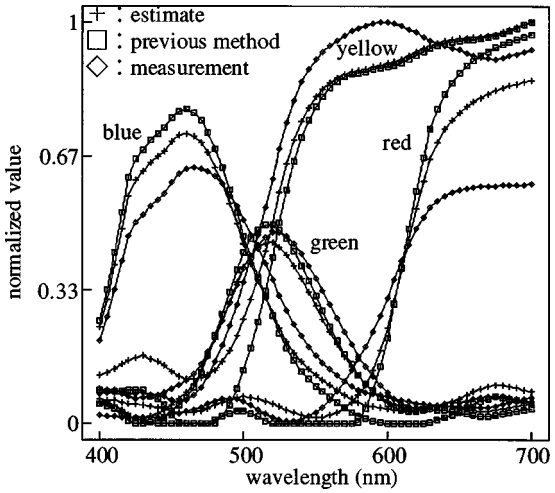

Fig. 11 Estimation results of surface-spectral reflectances.

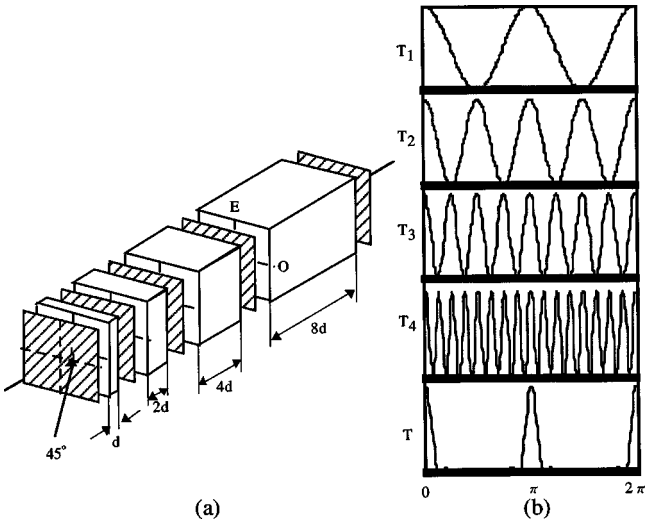

Fig. 12 Basic principle of the Lyot filter. (a) Structure and (b) filter outputs.

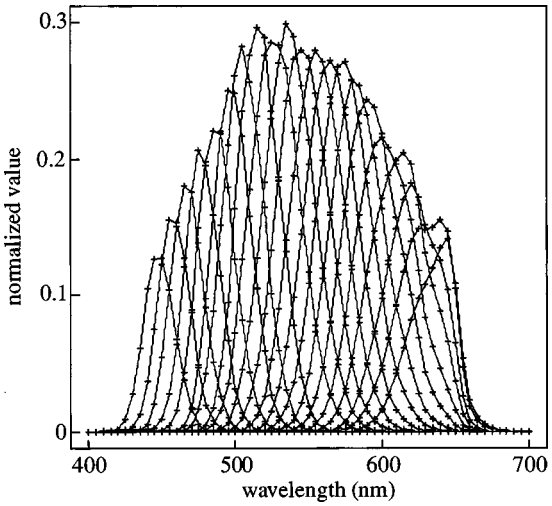

Fig. 14 Spectral-sensitivity functions of the camera using a liquid-crystal filter.

filter is convenient for spectral imaging because the wavelength band can be changed easily and electronically. That is, the center wavelength of filtration is electronically tunable with no moving parts. This filter is regarded as a type of polarization interference filter based on the design of the Lyot filter type.[17,18] Figure 12 shows the basic principle of the Lyot filter. It consists of several stages in sequence, each stage containing linear parallel polarizers sandwiching a liquid-crystal retarder (wave-plate) element. Each consecutive stage is operated in a higher order than the previous one. In Fig. 12(a), the optical axis E is parallel to the surfaces of the crystal retarders with thicknesses of d, $2d$, $4d$, and $8d$. The polarizers are inserted between retarders so that linearly polarized light impinges on a retarder at a 45° angle. Then, interference between two polarized light rays of ordinary and extraordinary yields a spectrally periodic transmission. Figure 12(b) shows the transmission at each stage in order of thickness from the thinnest retarder. The final output indicates a very narrow band.

Next, Fig. 13 depicts a single stage of a tunable liquid-crystal filter. The input polarizer splits the incoming light into equal components along the two crystal axes. Applying a voltage across the liquid-crystal retarder changes the index of refraction of one of the crystal axes. One light component is retarded relative to the other, thus creating a phase change. The output polarizer transmits light parallel to its transmission axis. Since the phase change depends on the wavelength, the liquid-crystal retarder selects which wavelengths are transmitted.

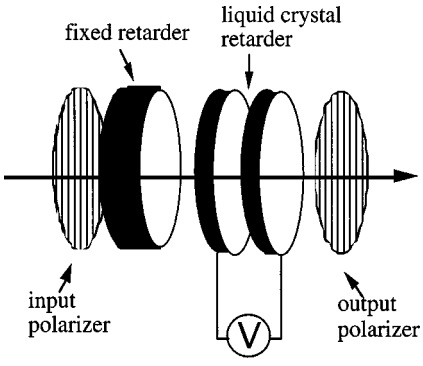

Fig. 13 Single stage of a tunable liquid-crystal filter.

This tunable liquid-crystal filter can be used in place of color filters in a multichannel camera system. The filter used in the present study has a 20 mm aperture and operates over the range 450–650 nm. We use the same monochrome CCD camera as the six-color camera system, and place this filter in front of the entrance lens of a C-mount. Figure 14 shows the whole spectral-sensitivity functions that were obtained by combining the filter transmittances and the spectral-sensitivity function of the monochrome CCD camera. The bandwidth of the spectral-sensitivity functions is about 50 nm. In order to estimate the illuminant and the surface-spectral reflectance functions of objects, the same algorithms presented in the previous sections can be applied to the high-dimensional image data acquired from this camera system.

8 Conclusion

The present paper has described a set of multichannel camera systems and algorithms for recovering both the surface-spectral-reflectance function and the illuminant spectral-power distribution from spectral imaging data. We have presented a camera system with six spectral channels of fixed wavelength bands. This system was created by using a monochrome CCD camera, a standard photographic lens, six different color filters, and a personal computer. The dynamic range of the camera was extended for sensing the high-intensity levels of highlights, and the spectral-sensitivity function of each sensor was measured precisely.

Object surfaces in a scene were supposed to be made of inhomogeneous dielectric materials, so that the reflection can be described by the dichromatic reflection model. Several algorithms were presented for estimating the spectral functions of illuminant and surface reflectance from the six-dimensional camera data. First, the spectral functions were represented by finite-dimensional linear models. Second, the illuminant parameters were estimated from the image

data for highlight parts within different objects. An algorithm was proposed for detecting highlight areas in the image. Third, the image was segmented into uniform surface regions, and the reflectance parameters of each region were estimated based on the two-dimensional histogram analysis. The reliability of the camera system and the algorithms was demonstrated in an experiment.

Moreover, we have proposed a multichannel camera system based on a new filtration mechanism using a tunable liquid-crystal filter. This filtration mechanism is convenient for spectral imaging because the filter bandwidth is narrower and the center wavelength is electronically tunable with no moving parts involved. This filter is a type of polarization interference filter. The same algorithms as used for the six-color camera system can be utilized to estimate the illuminant and surface-spectral function from the high-dimensional image data provided by this camera system. We are presently using the image data consisting of 21 channels in the visible wavelength.

The spectral functions of illuminant and surface-spectral reflectance were described by the linear finite-dimensional model. The model dimensions of $m=3$ for illuminant and $n=5$ for reflectance used in this paper were determined empirically. The model dimensions are bounded by the number of spectral channels. However, it should be noted that increasing the model dimension does not always make it easier to use the linear model nor does it improve estimation accuracy. The selection of the proper linear model dimension remains for future work.

Object surfaces were assumed to be composed of inhomogeneous dielectric materials. The proposed estimation algorithms have some limitations in their application to object surfaces. If the surfaces are fine textured, exhibit neutral color, or highlights do not occur, then our method is not applicable. However, if the spectral distribution of the illumination is known or can be measured directly using a spectrometer, then most limitations are removed and the application can be extended. For instance, surfaces of metals and papers, which are not described by the standard dichromatic reflection model, can be estimated from the image data. Moreover, then the method does not need to use highlights on any surface and is independent of object color.

References

1. B. A. Wandell, *Foundations of Vision*, Sinauer Associates, Sunderland, MA (1995).
2. S. Tominaga, ''Surface identification using the dichromatic reflection model,'' *IEEE Trans. Pattern. Anal. Mach. Intell.* **13**, 658–670 (1991).
3. Y. Miyake and Y. Yokoyama, ''Obtaining and reproduction of accurate color images based on human perception,'' *SPIE Color Imaging: Device-Independent Color, Color Hardcopy, and Graphics Arts III, Proc. SPIE* **3300**, 190–197 (1998).
4. R. Hall, *Illumination and Color in Computer Generated Imagery*, Springer-Verlag, Berlin (1989).
5. S. Tominaga, ''A multi-channel vision system for estimating surface and illuminant functions,'' *J. Opt. Soc. Am. A* **13**, 2163–2173 (1996).
6. S. Tominaga, ''Computational approach and a multi-channel vision System,'' *Proc. of the 8th Congress of the International Colour Association*, pp. 71–76 (1997).
7. G. J. Klinker, S. A. Shafer, and T. Kanade, ''The measurement of highlights in color images,'' *Int. J. Comput. Vis.* **2**, 7–32 (1988).
8. S. Tominaga and B. A. Wandell, ''The standard surface reflectance model and illuminant estimation,'' *J. Opt. Soc. Am. A* **6**, 576–584 (1989).
9. D. B. Judd, *et al.*, ''Spectral distribution of typical daylight as a function of correlated color temperature,'' *J. Opt. Soc. Am.* **54**, 1031–1040 (1964).
10. L. T. Maloney, ''Evaluation of linear models of surface spectral reflectance with small numbers of parameters,'' *J. Opt. Soc. Am. A* **3**, 1673–1683 (1986).
11. M. J. Vrhel, *et al.*, ''Measurement and analysis of object reflectance spectra,'' *Color Res. Appl.* **19**, 4–9 (1994).
12. S. Tominaga, ''Surface reflectance estimation by the dichromatic model,'' *Color Res. Appl.* **21**, 104–114 (1996).
13. L. T. Maloney and B. A. Wandell, ''Color constancy: A method for recovering surface spectral reflectance,'' *J. Opt. Soc. Am. A* **3**, 29–33 (1986).
14. D. H. Brainard and W. T. Freeman, ''Bayesian color constancy,'' *J. Opt. Soc. Am. A* **14**, 1393–1411 (1997).
15. S. Tominaga and B. Wandell, ''Component estimation of surface spectral reflectance,'' *J. Opt. Soc. Am. A* **7**, 312–317 (1990).
16. S. Tominaga, ''Color classification of natural color images,'' *Color Res. Appl.* **17**, 230–239 (1992).
17. P. Miller, ''Tunable narrowband birefringent filters for astronomical imaging,'' *Proc. SPIE* **1235**, 466 (1990).
18. P. Foukal, P. Miller, and C. Hoyt, ''Liquid crystal tunable light filters for surveillance and remote sensing applications,'' *Proc. SPIE* **1952**, 168–177 (1993).

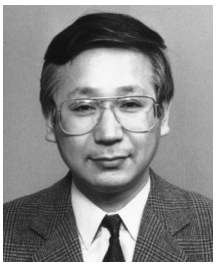

Shoji Tominaga received his BE, MS, and PhD degrees in electrical engineering from Osaka University, Toyonaka, Osaka, Japan, in 1970, 1972, and 1975, respectively. From 1975 to 1976, he was with the Electrotechnical Laboratory, Osaka. Since 1976, he has been with Osaka Electro-Communication University, Neyagawa, Osaka, where he is currently a professor with the Department of Engineering Informatics. During the 1987–1988 academic year he was a visiting scholar at the Department of Psychology, Stanford University. His research interests include computational color vision, color image analysis, and neural networks. He is a member of OSA, SPIE, IEEE, ACM, SID, and IS&T.